Nanoporous silicon multilayers for terahertz filtering

Shu-Zee A. Lo* **and Thomas E. Murphy**

Department of Electrical and Computer Engineering, University of Maryland, College Park, Maryland 20742, USA
**Corresponding author: alenciou@umd.edu*

Received July 21, 2009; revised August 18, 2009; accepted August 20, 2009;
posted August 25, 2009 (Doc. ID 113473); published September 18, 2009

We describe the fabrication, simulation, and measurement of a terahertz (THz) filter composed of nanoporous silicon multilayers. Using electrochemical etching, we fabricated a structure composed of alternating high- and low-index layers that achieves 93% power reflectivity at the target wavelength of 1.17 THz, with a stopband of 0.26 THz. The measured reflection and transmission spectra of the multilayer filter show excellent agreement with calculations based on the refractive indices determined separately from single-layer measurements. This technique could provide a convenient, flexible, and economical way to produce THz filters, which are essential in a variety of future applications. © 2009 Optical Society of America

OCIS codes: 220.0220, 220.4241, 230.1480, 230.7408, 300.6495.

While there have been significant advances in techniques to generate and detect terahertz (THz) signals, there have been comparatively few reports of structures that manipulate and control them. In particular, THz bandpass filters could be essential components in THz spectroscopy, imaging, and quantum cascade lasers. Optical bandpass filters typically employ multilayer film deposition techniques that cannot be easily applied in the THz regime because of the much larger wavelength scale and scarcity of sufficiently transparent dielectric materials.

Several techniques have been used to fabricate THz multilayer filters, including stacking and assembly of semiconductor wafers [1–5], ceramics [6–8], plastic films [9,10] and other dielectrics, or pressed and extruded polymer laminates [11,12]. Thick film sputter-deposition methods have also been used to fabricate multilayers of silicon, oxides, and other semiconductors [13,14]. Polymer nanoparticle composites have been used to provide additional flexibility in controlling the effective refractive index at THz frequencies [12], and liquid crystals have been used in conjunction with stacked layers to achieve electrical tenability [15].

We report here a flexible and economical method to build THz multilayers using nanoporous silicon. Nanoporous silicon is an easily fabricated nanoscale composite of air and silicon that has been shown to be suitable for THz transmission [16–18]. Compared with earlier approaches, our technique avoids the difficulty associated with stacking and assembly of dielectric layers, eliminates the need for lengthy deposition of thick films, and permits a wide range of refractive indices to be fabricated from a single silicon substrate. The nanoporous nature of the resulting structure would allow for incorporation of liquids and gases directly into the films, and the large surface area to volume ratio is attractive for sensor applications that rely on selective binding to an activated surface.

The porous silicon multilayers were fabricated using electrochemical etching, starting from heavily boron-doped ($\rho=1-5\ \mathrm{m}\Omega\ \mathrm{cm}$, $N\sim10^{20}\ \mathrm{cm}^{-3}$) p-type silicon wafers. The etching was performed using an electrochemical cell, in which the bulk silicon wafer is clamped between two chambers, each filled with an electrolyte composed of hydrofluoric acid, water, and ethanol in volume ratio of 1:1:2. The etching current was applied through immersed platinum electrodes, using a computer-controlled galvanostat. The diameter of the etched region was 10 mm, which is defined by an O-ring aperture in the electrochemical cell. The degree of porosity (and hence the refractive index) is related to the electrochemical current density, which is controlled by a computer. Etching occurs only at the interface between the bottom porous layer and the silicon substrate, leaving all of the overlying layers intact. After calibrating the etch rate and porosity using single-layer samples, more complicated multilayer structures can be fabricated by changing the anodization current as a function of time while etching [19].

To characterize the dielectric properties of porous silicon, we first fabricated single-layer samples with low and high porosities. For the low-porosity sample, we used a current density of 18 $\mathrm{mA/cm^2}$. The current was applied in 100 ms pulses with a 300 ms pause in between current pulses to allow the electrolyte concentration to equilibrate in the pores. Gravimetric measurements gave a porosity of 40% and a net etch rate of 0.3 μm/min under these conditions. The sample was etched to a total depth of 285 μm, after which a strong current pulse (226 $\mathrm{mA/cm^2}$ for 7 s) was applied, causing the porous layer to separate from the substrate, yielding a free-standing porous membrane. This process was repeated with a current density of 90 $\mathrm{mA/cm^2}$ to produce a second membrane with a porosity of 62%, etch rate of 1.0 μm/min, and total thickness of 285 μm. Following the etching process, the porous membranes were rinsed in isopropyl alcohol and air dried. The porous layers were partially oxidized by rapid thermal annealing for 5 min. at 400°C in an ambient environment, which leads to

 © 2009 Optical Society of America

an improvement of the long-term stability and reduced THz absorption [18].

The transmission spectra of the single-layer porous membranes were measured using a conventional THz time-domain spectroscopy system comprising an InAs semiconductor emitter [20] and ZnTe electro-optic detector [21]. The THz beam was collimated and focused to a 1 mm diameter spot on the sample using a pair of off-axis parabolic mirrors, and then directed to the electro-optic detector through a complementary set of optics. Figures 1(a) and 1(b) show the THz transmission spectra for the low- and high-porosity samples, respectively. The Fabry–Pérot fringes seen in the transmission spectra are caused by internal reflections within the porous silicon layer, and the excess loss at higher frequencies could be attributed to a phonon absorption tail, similar to that seen in crystalline silicon [22]. Our experimental measurements are thought to span only the low-frequency tail of this absorption feature, where the relative dielectric permittivity can be approximated by

$$\epsilon_r(\omega) = A + iB\omega, \tag{1}$$

with free parameters A and B that relate to the absorption strength and resonant frequency.

The theoretical transmission spectrum of a free-standing dielectric layer at normal incidence, including the effect of multiple internal reflections, is given by [23]

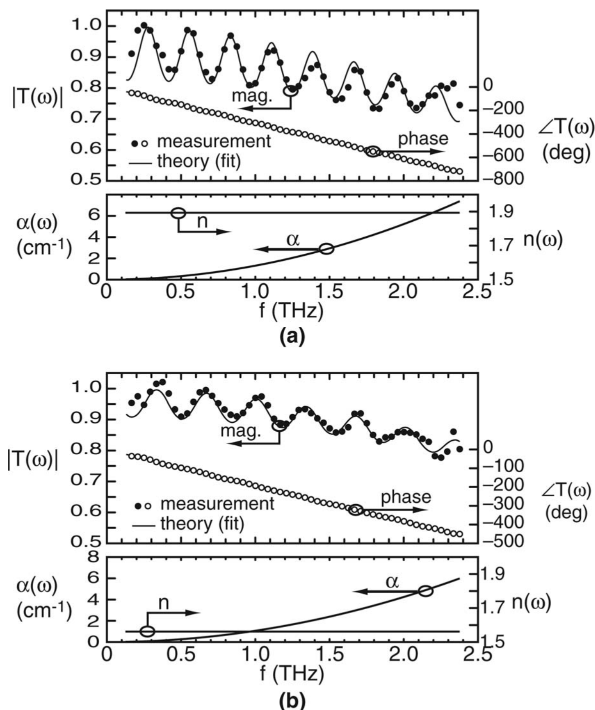

Fig. 1. Measured and theoretical THz transmission spectrum for free-standing single-layer porous silicon samples fabricated with (a) low and (b) high porosity. The theoretical curves were obtained by fitting Eq. (2) to the experimental observations, using the index model given in Eq. (1). The refractive indices and attenuation coefficients determined from the theoretical fits are shown directly below the corresponding transmission spectra.

$$T(\omega) = \frac{4\tilde{n}}{(\tilde{n}+1)^2} \frac{e^{i(\tilde{n}-1)\omega d/c}}{1-\left(\dfrac{\tilde{n}-1}{\tilde{n}+1}\right)^2 e^{i2\tilde{n}\omega d/c}}, \tag{2}$$

where $\tilde{n}(\omega) \equiv \sqrt{\epsilon_r(\omega)}$ is the complex index of refraction, which implicitly depends on frequency as described in Eq. (1).

For each of the single-layer samples, the two free parameters A and B were determined by performing a weighted nonlinear least-squares fit of Eq. (2) to the experimentally measured transmission spectrum, using the film thickness d obtained from independent measurements. The solid curves in Figs. 1(a) and 1(b) indicate the best fit theoretical transmission function for the low- and high-porosity samples, showing excellent matching to the experimental measurements. Directly below each transmission spectrum, we plot the corresponding calculated loss coefficient α and refractive index n. The refractive indices are approximately 1.89 and 1.56 for the low- and high-porosity samples, respectively, and show little dispersion over the frequency range of interest. The residual losses could potentially be reduced by optimizing the dopant concentration, porosity, and pore size.

The Bragg grating filter was fabricated by periodically switching the current density between 90 and 18 mA/cm^2, to form a 13-layer sample composed of alternating high- and low-porosity regions. Rather than lifting off the etched layers using a strong current pulse, as was done for the single-layer films, we etched through the entire wafer, stopping when the electrochemical cell exhibited strong conduction between the two chambers. Following the fabrication, the rear surface was reactive-ion etched for a short time in a CF_4/O_2 plasma to remove any residual crystalline silicon from the back side.

Figure 2 is a scanning electron micrograph showing the cross-section of the completed device. The thickness of each layer was designed to be $\lambda/4n$, where n is the refractive index of the layer and λ is the desired center wavelength of the filter, chosen here to be 256 μm (1.17 THz).

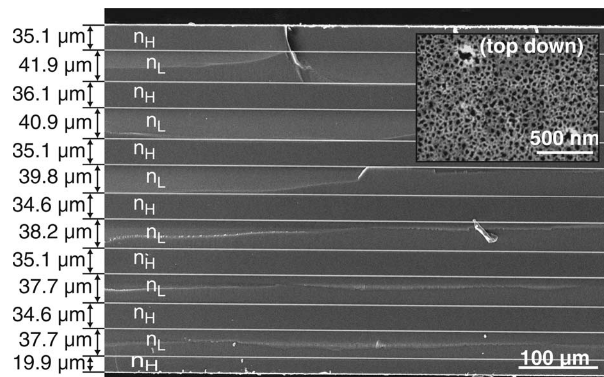

Fig. 2. Cross-sectional scanning electron micrograph of a 13-layer porous silicon Bragg grating filter, composed of alternating high and low refractive index layers. Inset, top-down scanning electron micrograph showing nanoscale structure of porous material.

Figure 3(a) plots the measured THz transmission (magnitude and phase) for the multilayer Bragg filter, showing a clear decrease in transmission for a band of frequencies centered about the target frequency of 1.17 THz. The complementary reflection spectrum is shown in Fig. 3(b). The reflection spectrum was measured with *p* polarization at a 20° angle of incidence, which causes a slight blueshift in the center frequency compared to the normal-incidence case. When performing the reflection measurements, the reflected signal from the filter was compared to a reference signal obtained by replacing the Bragg filter with a silver mirror with nearly perfect reflectivity.

The solid curves plotted in Fig. 3 indicate the theoretically calculated transmission and reflection spectra, which exhibit excellent agreement with the experimental measurements. The theoretical spectra were calculated using the dielectric parameters obtained separately from single-layer measurements (Fig. 1), and the layer thicknesses determined from cross-sectional microscopy (Fig. 2.) The reflection spectrum was calculated to have less than 1.5 ps of group-delay variation across the 0.26 THz stopband, which is sufficiently small for communication applications [24].

These results demonstrate that porous silicon could be a convenient and inexpensive platform for building multilayer THz devices. Even though the porous silicon films are etched from a highly doped crystalline silicon substrate, the resulting structures exhibit low absorption loss over a wide range of THz frequencies. While the Bragg filter presented here used only two different porosities, in principle one could construct arbitrary refractive index profiles by simply adjusting the anodization current density as a function of time. This could enable more complex filters, cavities, antireflection coatings, and even graded-index dielectric waveguides.

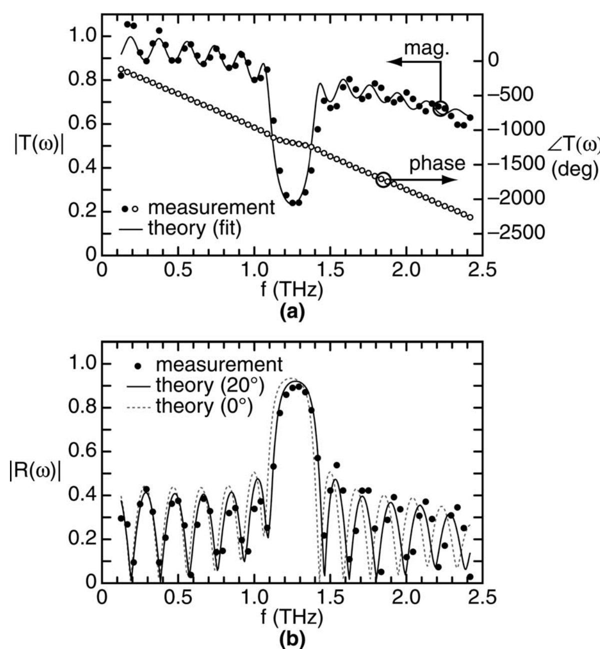

Fig. 3. THz transmission and reflection spectra of a porous silicon Bragg filter. The solid curves indicate a theoretical calculation based on the measured film thicknesses and separately measured layer properties.

This work is supported by the National Science Foundation (NSF) CAREER award 0546928 and NSF CBET award 0932673. The work was performed in part at the University of Maryland Nanocenter. The authors thank A. M. Rossi, A. Giovannozzi, and P. Apiratikul for advice and assistance in this work.

References

1. R. Schiwon, G. Schwaab, E. Brundermann, and M. Havenith, Appl. Phys. Lett. **83**, 4119 (2003).
2. N. Krumbholz, K. Gerlach, F. Rutz, and M. Koch, Appl. Phys. Lett. **88**, 202905 (2006).
3. H. Němec, P. Kužel, F. Garet, and L. Duvillaret, Appl. Opt. **43**, 1965 (2004).
4. T. W. Du Bosq, A. V. Muravjov, R. E. Peale, and C. J. Fredricksen, Appl. Opt. **44**, 7191 (2005).
5. W. Withayachumnankul, B. M. Fischer, and D. Abbott, Opt. Commun. **281**, 2374 (2008).
6. H. Němec, P. Kužel, L. Duvillaret, A. Pashkin, M. Dressel, and M. T. Sebastian, Opt. Lett. **30**, 549 (2005).
7. N. Matsumoto, T. Nakagawa, K. Kageyama, N. Wada, and Y. Sakabe, Jpn. J. Appl. Phys. Part 1 **45**, 7499 (2006).
8. F. Rutz, M. Koch, L. Micele, and G. de Portu, Appl. Opt. **45**, 8070 (2006).
9. J. Shao and J. A. Dobrowolski, Appl. Opt. **32**, 2361 (1993).
10. D. Turchinovich, A. Kammoun, P. Knobloch, T. Dobbertin, and M. Koch, Appl. Phys. A **74**, 291 (2002).
11. S. Wietzke, C. Jansen, F. Rutz, D. Mittleman, and M. Koch, Polym. Test. **26**, 614 (2007).
12. J. Lott, C. Xia, L. Kosnosky, C. Weder, and J. Shan, Adv. Mater. **20**, 3649 (2008).
13. J. S. Seeley, R. Hunneman, and A. Whatley, Appl. Opt. **20**, 31 (1981).
14. I. Hosako, Appl. Opt. **44**, 3769 (2005).
15. R. Wilk, N. Vieweg, O. Kopschinski, and M. Koch, Opt. Express **17**, 7377 (2009).
16. S. Labbé-Lavigne, S. Barret, F. Garet, L. Duvillaret, and J.-L. Coutaz, J. Appl. Phys. **83**, 6007 (1998).
17. S. Ramani, A. Cheville, E. Garcia, and V. Agarwal, Phys. Status Solidi C **4**, 2111 (2007).
18. S.-Z. A. Lo, A. M. Rossi, and T. E. Murphy, Phys. Status Solidi A **206**, 1273 (2009).
19. M. G. Berger, C. Dieker, M. Thönissen, L. Vescan, H. Lüth, H. Münder, W. Theiss, M. Wernke, and P. Grosse, J. Phys. D **27**, 1333 (1994).
20. J. N. Heyman, P. Neocleous, D. Hebert, P. A. Crowell, T. Müller, and K. Unterrainer, Phys. Rev. B **64**, 085202 (2001).
21. A. Nahata, A. S. Weling, and T. F. Heinz, Appl. Phys. Lett. **69**, 2321 (1996).
22. J. Dai, J. Zhang, W. Zhang, and D. Grischkowsky, J. Opt. Soc. Am. B **21**, 1379 (2004).
23. L. Duvillaret, F. Garet, and J.-L. Coutaz, IEEE J. Sel. Top. Quantum Electron. **2**, 739 (1996).
24. I. A. Ibraheem, N. Krumbholz, D. Mittleman, and M. Koch, IEEE Microw. Wirel. Compon. Lett. **18**, 67 (2008).